Geophys. J. Int. (2008) doi: 10.1111/j.1365-246X.2008.03974.x

M_{wpd}: a duration–amplitude procedure for rapid determination of earthquake magnitude and tsunamigenic potential from *P* waveforms

Anthony Lomax[1] and Alberto Michelini[2]

[1] *ALomax Scientific, Mouans-Sartoux, France. E-mail: anthony@alomax.net*
[2] *Istituto Nazionale di Geofisica e Vulcanologia, Roma, Italy*

Accepted 2008 September 13. Received 2008 September 11; in original form 2007 October 3

SUMMARY

We present a duration–amplitude procedure for rapid determination of a moment magnitude, M_{wpd}, for large earthquakes using *P*-wave recordings at teleseismic distances. M_{wpd} can be obtained within 20 min or less after the event origin time as the required data are currently available in near real time. The procedure determines apparent source durations, T_0, from high-frequency, *P*-wave records, and estimates moments through integration of broad-band displacement waveforms over the interval t_P to $t_P + T_0$, where t_P is the *P*-arrival time. We apply the duration–amplitude methodology to 79 recent, large earthquakes (global centroid-moment-tensor magnitude, $M_{\rm w}^{\rm CMT}$, 6.6–9.3) with diverse source types. The results show that a scaling of the moment estimates for interplate thrust and possibly tsunami earthquakes is necessary to best match $M_{\rm w}^{\rm CMT}$. With this scaling, M_{wpd} matches $M_{\rm w}^{\rm CMT}$ typically within ± 0.2 magnitude units, with a standard deviation of $\sigma = 0.11$, equaling or outperforming other approaches to rapid magnitude determination. Furthermore, M_{wpd} does not exhibit saturation; that is, for the largest events, M_{wpd} does not systematically underestimate $M_{\rm w}^{\rm CMT}$. The obtained durations and duration–amplitude moments allow rapid estimation of an energy-to-moment parameter Θ^* used for identification of tsunami earthquakes. Our results show that $\Theta^* \leq -5.7$ is an appropriate cut-off for this identification, but also show that neither Θ^* nor $M_{\rm w}$ is a good indicator for tsunamigenic events in general. For these events, we find that a reliable indicator is simply that the duration T_0 is greater than about 50 s. The explicit use of the source duration for integration of displacement seismograms, the moment scaling and other characteristics of the duration–amplitude methodology make it an extension of the widely used, M_{wp}, rapid magnitude procedure. The need for a moment scaling for interplate thrust and possibly tsunami earthquakes may have important implications for the source physics of these events.

Key words: Tsunamis; Earthquake dynamics; Earthquake source observations; Seismic monitoring and test-ban treaty verification; Body waves; Wave propagation.

INTRODUCTION

Effective tsunami warning and emergency response for large earthquakes requires accurate knowledge of the event size within 30 min or less after the event origin time (OT). The 2004 December 26, *M* 9 Sumatra–Andaman earthquake caused a tsunami that devastated coasts around the Eastern Indian Ocean within 3 hr; the 2006 July 17, *M* 7.7 Java earthquake caused an unexpectedly large and destructive tsunami. For both events, the magnitudes available within the first hour after the event OT severely underestimated the event size (Kerr 2005; PTWC 2006a,b).

Currently, the earliest, accurate estimates of the size of major and great earthquakes come from long-period, moment-tensor determinations, including the authoritative, global centroid-moment-tensor (CMT) determination and corresponding moment magnitude, $M_{\rm w}^{\rm CMT}$ (Dziewonski *et al.* 1981; Ekström 1994), and related procedures (e.g. Kawakatsu 1995). These estimates are based on seismic *S* and surface wave waveform recordings, typically not available until an hour or more after OT. Other, more rapid moment-tensor based estimates tend to underestimate the size of great earthquakes, as we discuss below.

Another procedure based on surface waves is the mantle magnitude, $M_{\rm m}$, (Okal & Talandier 1989; Newman & Okal 1998; Weinstein & Okal 2005). The spectral amplitude of mantle Rayleigh waves at variable periods (between 50 and 300 s for large events), combined with approximate corrections for geometrical spreading and Rayleigh wave excitation at the source, gives the $M_{\rm m}$ estimate and a corresponding moment. $M_{\rm m}$ is potentially available within minutes after the first Rayleigh wave passage (i.e. about 20 min after OT at 30° great-circle distance (GCD), and about 50 min after OT at 90° GCD), but for very large events the analysis of waves at increased periods (450 s or more) may be required (UNESCO 2005; Weinstein & Okal 2005) leading to an increased delay after OT for obtaining the $M_{\rm m}$ estimate.

Seismic *P* waves are the first signals to arrive at seismic recording stations. At teleseismic distances (30°–90° GCD), the arrival times of the initial *P* wave are used routinely to locate the earthquake hypocentre within about 10–15 min after OT. The initial *P*-waves and following *P*-wave train also contain comprehensive information about the event size and source character. Boatwright & Choy (1986) show that the total radiated seismic energy can be estimated from the *P* waves alone.

There are a number of procedures for rapid analysis of large earthquakes using seismic *P* waves currently in use at earthquake and tsunami monitoring centres. Because these procedures use only the *P*-wave portion of a seismogram, event size estimates are potentially available only a few minutes after the *P* waveform has been recorded at teleseismic distances, that is, in as little as 10–15 min after OT at 30° GCD, and about 20 min after OT at 90° GCD.

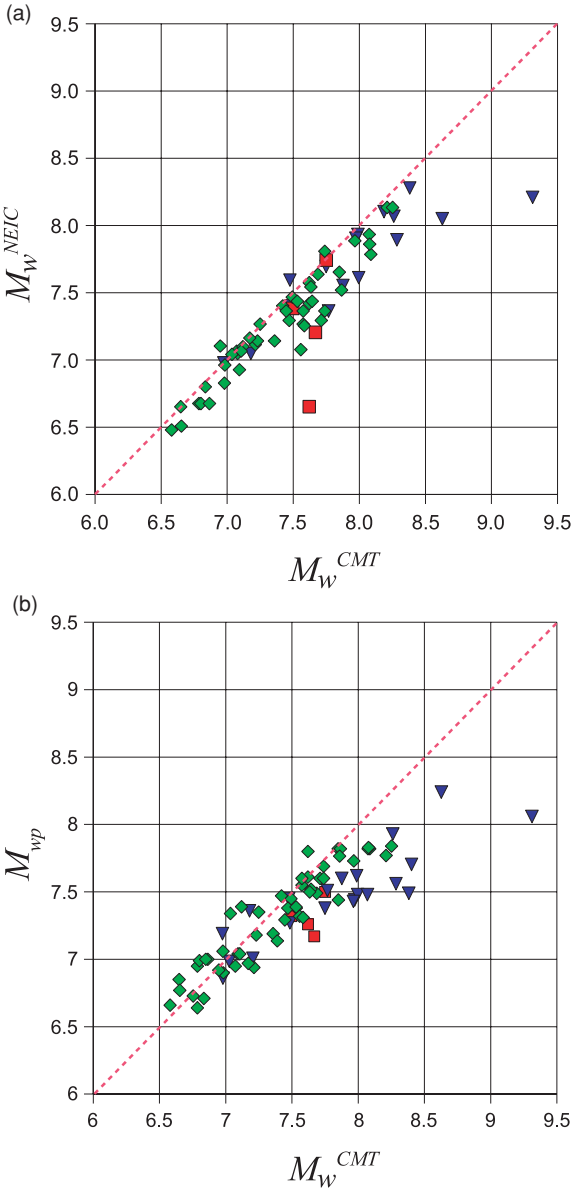

Figure 1. Moment magnitudes from rapid analysis methods using seismic *P* waves compared to CMT magnitude M_w^{CMT} for the studied events (Table 1, Fig. 4). (a) M_w^{NEIC} from the NEIC Fast Moment-Tensor procedure (Sipkin 1994; http://earthquake.usgs.gov); (b) M_{wp} from this study, determined following the procedure described by Tsuboi (2000), Hirshorn (2006) and Lomax *et al*. (2007); (c) M_{wp} from this study with magnitude-dependent correction of Whitmore *et al.* (2002). Event symbols are: interplate thrust events (blue inverted triangles); tsunami earthquakes (red squares); other event types (green diamonds). In this and the following figures, the value $M_w^{CMT} = 9.3$ for 2004.12.26 Sumatra–Andaman is from Tsai *et al.* (2005).

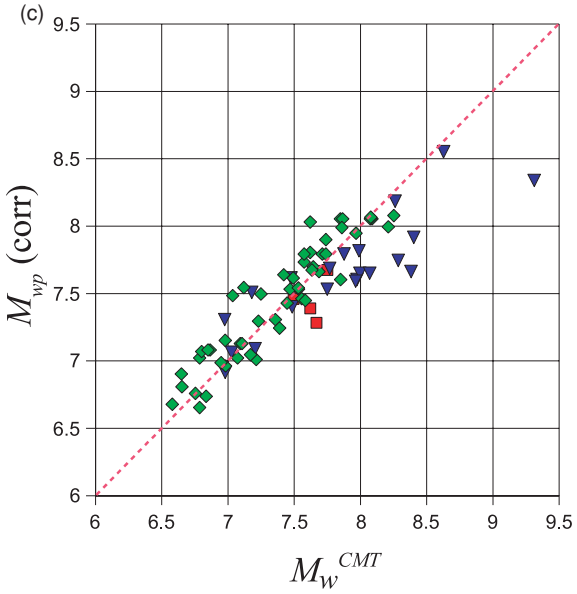

Figure 1. (*Continued.*)

One of these procedures is the U.S. Geological Survey National Earthquake Information Center (NEIC) Fast Moment Tensor (Sipkin 1994; http://earthquake.usgs.gov) which produces an estimate of the seismic moment tensor and moment magnitude, M_w^{NEIC}, for earthquakes of magnitude of 5.5 or greater within the order of 30 min after OT through automated processing and inversion of *P*-wave waveforms.

Another *P*-wave procedure is the widely used, M_{wp} moment-magnitude algorithm (Tsuboi *et al.* 1995, 1999; Tsuboi 2000) which considers very-broad-band, *P*-wave displacement seismograms as approximate far-field, source-time functions. These displacement seismograms are integrated and corrected approximately for geometrical spreading and an average radiation pattern to obtain scalar moments at each station. Application of the standard moment-magnitude formula, averaging over stations and optionally applying a magnitude-dependent correction (Whitmore *et al.* 2002) gives a moment magnitude, M_{wp}, for an event.

M_w^{NEIC} and M_{wp} match closely M_w^{CMT} up to $M_w^{CMT} \approx 7.5$, but at greater magnitudes they tend to increasingly underestimate M_w^{CMT} (Fig. 1, Table 1). To resolve this magnitude saturation problem while providing accurate and rapid magnitude estimates for large earthquakes, a number of authors have proposed new methodologies for magnitude determination based on *P*-wave signals.

Menke & Levin (2005) propose that the ratio of long-period, *P*-wave displacement amplitudes between a target event and a nearby reference event of known size can rapidly provide the magnitude of the target event. Lockwood & Kanamori (2006) show that wavelet analysis of *P* waves distinguishes a significantly greater amplitude of the long-period, *W*-phase for the 2004 December 26, *M* 9 Sumatra–Andaman relative to the *W*-phase of the 2005 March 28, *M* 8.6 Northern Sumatra earthquakes (The *W*-phase is a superposition of Rayleigh wave overtones that arrive before the *S* wave). They propose that such analysis can be used for rapid identification of the largest, great earthquakes and their high tsunamigenic potential.

Bormann & Wylegalla (2005), Bormann *et al.* (2006) and Bormann & Saul (2008) calculate a cumulative m_B magnitude, m_{Bc}, by summing the peak velocity amplitudes for major signal pulses between consecutive zero crossings in the *P* waveform. Hara (2007) combines measures of the high-frequency duration and maximum displacement amplitude of *P* waveforms for a set of large, shallow earthquakes to determine an empirical relation for moment magnitude.

Lomax (2005) shows for very large earthquakes that the location of the end of rupture, and thus an estimate of the event size, can be rapidly determined from measures of the *P*-wave duration on high-frequency records. Lomax & Michelini (2005) note that the ratio of the high-frequency, *P*-wave durations from the 2004, *M* 9 Sumatra–Andaman and the 2005, *M* 8.6 Northern Sumatra earthquakes matches the ratio of the CMT moment values for the two events, and suggest that the high-frequency, *P*-wave duration could be used for rapid magnitude estimation for individual events. Lomax *et al.* (2007) use teleseismic (GCD $\geq 30^\circ$), *P*-wave signals to estimate radiated seismic energy, E, and source duration, T_0, and show that an 'energy–duration' moment relation, $M_0^{ED} \propto E^{1/2} T_0^{3/2}$, based on an expression for E from Vassiliou & Kanamori (1982), gives a moment magnitude, M_{ED}, that matches closely M_w^{CMT} for a set of recent, large earthquakes.

These new methodologies for rapid magnitude determination based on *P*-wave signals all produce useful magnitude estimates, M^{est}, for very large earthquakes. Most of these methodologies, however, show significant differences with M_w^{CMT} (i.e. $|M^{est} - M_w^{CMT}| \geq 0.3$) for many events, including some of the most important and destructive interplate thrust events and tsunami earthquakes (tsunami earthquakes are characterized by unusually large tsunamis and a deficiency in moment release at high frequencies, e.g. Kanamori 1972; Polet & Kanamori 2000; Satake 2002). Most of these methodologies also give $\Delta M = M^{est} - M_w^{CMT}$ values which change systematically with increasing M_w^{CMT}; this effect is equivalent to the magnitude saturation of M_w^{NEIC} and M_{wp}.

To further investigate and resolve these problems, we introduce here a rapid and robust, 'duration–amplitude' procedure to obtain an earthquake moment and a moment magnitude, M_{wpd}, from *P*-wave recordings at teleseismic distances. This procedure first determines apparent source durations, T_0, from high-frequency, *P*-wave records, and then estimates moments through integration of broadband displacement records over the interval t_P to $t_P + T_0$, where t_P is the *P*-arrival time. This methodology can be viewed as an extension of the M_{wp} moment-magnitude algorithm.

THEORETICAL DEVELOPMENT AND CALIBRATION OF THE DURATION–AMPLITUDE PROCEDURE

Basic theory

Given the far-field, *P*-displacement $u(t)$, for an earthquake source of rupture duration, T_0, a well-established theoretical expression for the scalar, seismic moment, M_0, is

$$M_0 = C_M \int_{t_P}^{t_P+T_0} u(t)\mathrm{d}t, \tag{1}$$

where t_P is the *P*-arrival time, $u(t)$ is corrected for geometrical spreading and attenuation and C_M is a constant that depends on the density and wave speed at the source and station, a double-couple radiation pattern and other factors (e.g. Aki & Richards 1980; Boatwright & Choy 1986; Tsuboi *et al.* 1995; Newman & Okal 1998; Kanamori & Rivera 2004; see Appendix A for details). Eq. (1) suggests that the scalar moment, M_0, of an earthquake can be determined from *P*-wave displacement seismograms. Application of the standard moment-magnitude formula to the obtained M_0,

$$M_w = \left(\log_{10} M_0 - 9.1\right)/1.5, \tag{2}$$

(Hanks & Kanamori 1979; Bormann 2002) gives a *P*-wave estimate of the moment magnitude, M_w, for an event.

Eq. (1) cannot be used directly to obtain accurate moment estimates for a number of reasons, including the presence of surface reflected and other secondary phases, and the difficulty of estimating T_0. The M_{wp} magnitude procedure addresses some of these problems by estimating the scalar moment from the larger of the first peak or the first peak-to-peak amplitudes on *P*-displacement seismograms integrated using eq. (1), though the integral is performed without explicit knowledge or use of T_0 (e.g. Tsuboi *et al.* 1999).

To make further use of eq. (1) to obtain more accurate, rapid moment-magnitude estimates, we begin by examining moments, $\hat{M}_0$, and magnitudes, M_{wpd}, determined through application to teleseismic *P*-wave ground-displacement seismograms of a modified form of eq. (1),

$$\hat{M}_0 = kC_M \mathrm{Max}\left[\int_{t_P}^{t_P+T_0} u^+(t)\,\mathrm{d}t, \int_{t_P}^{t_P+T_0} u^-(t)\,\mathrm{d}t\right]. \tag{3}$$

The modifications in eq. (3) includes the following: (1) The integral in eq. (1) is taken separately over the positive, $u^+(t)$, and the absolute value of negative, $|u^-(t)|$, displacement amplitudes to help separate the direct *P* waves from surface reflection phases and other phases with opposite polarity; the maximum of these two integrals is used to calculate the moment estimate. (2) A constant, k, is included to compensate for unknown errors and biases in the terms of C_M and in the correction of $u(t)$ for attenuation and geometrical spreading (if C_M and the corrections were physically exact, a value of $k = 1$ would be expected). In addition, the source duration, T_0, is estimated through measures on high-frequency, *P*-wave seismograms (Lomax 2005; Lomax et al. 2007) and explicitly used to define the upper limit of integration. Application of the standard moment-magnitude formula, eq. (2), using $\hat{M}_0$ and averaging over stations using robust statistics (20 per cent trimmed mean) gives a *P*-wave moment magnitude, M_{wpd}, for an event.

Further details on this procedure are given in Appendices A–C; the processing steps are illustrated in Fig. 2. We note here that the amplitude correction of the displacement waveforms for attenuation and geometrical spreading and the calculation of C_M make use of the PREM model (Dziewonski & Anderson 1981) without a crust (hereinafter referred to as PREM_NC), since most large events occur in oceanic regions. For shallow continental events, the effect of the crust on C_M is introduced as a magnitude correction using the PREM properties for the lower crust. Also, the radiation pattern factor in C_M for strike-slip events, which differs greatly from that for all other event types, is determined empirically. Table 1 indicates the classification of each event according to source type and oceanic versus continental setting, mainly based on event information from the NEIC (http://earthquake.usgs.gov) and the global CMT catalogue (http://www.globalcmt.org). This classification takes into account the epicentre, depth and moment-tensor mechanism in relation to the background seismicity and the surrounding tectonic plates and plate boundaries; in a few cases additional information from the NEIC tectonic summary is used.

Our use in eq. (3) of the maximum of the integrals over positive and negative *P*-displacement is a direct extension to all peaks in

Table 1. Events used in this study and duration–amplitude results.

		NEIC					CMT			This study		This study, duration–amplitude results				
Origin time	Event	Type[a]	Latitude (°)	Longitude (°)	Depth (km)	M_w^{NEIC}	Depth (km)	T_0[b]	M_w^{CMT}	M_{wp}	M_{wp} Corr[c]	T_0 (s)	M_{wpd}	Moment scaled	M_{wpd} scaling	θ^*
1992.09.02 00:15	Nicaragua	T	11.74	−87.34	44	6.7	15	89	7.6	7.3	7.4	222	7.5	Yes	7.6	−6.9
1992.12.12 05:29	Flores Indonesia	P	−8.48	121.90	49	7.4	20	45	7.7	7.7	7.9	100	7.7		7.7	−5.7
1993.07.12 13:17	Hokkaido	P	42.85	139.20	18	7.3	17	50	7.7	7.6	7.8	87	7.8		7.8	−5.4
1994.01.17 12:30	S California	R	34.21	−118.54	21	6.7	17	16	6.6	6.9	6.9	15	6.7		6.7	−4.8
1994.06.02 18:17	Java	T	−10.48	112.84	6	7.7	15	78	7.7	7.5	7.7	108	7.5	Yes	7.7	−5.9
1994.06.09 00:33	Bolivia	D	−13.84	−67.55	631	8.1	647	58	8.2	7.8	8.0	42	8.2		8.2	−3.9
1994.10.04 13:23	Kuril Islands	P	43.77	147.32	61	8.1	68	60	8.3	7.8	8.1	67	8.2		8.2	−4.5
1995.07.30 05:11	Chile	I	−23.34	−70.29	9	7.9	29	67	8.0	7.6	7.8	101	7.8	Yes	8.0	−5.2
1995.10.09 15:35	Mexico	I	19.06	−104.21	4	7.9	15	66	8.0	7.4	7.6	77	7.6	Yes	7.8	−5.2
1995.12.03 18:01	Kuril Islands	I	44.66	149.30	23	7.6	26	57	7.9	7.6	7.8	61	7.6	Yes	7.8	−5.0
1996.02.17 05:59	Irian Jaya	I	−0.89	136.95	11	8.1	15	66	8.2	N/A	N/A	112	7.8	Yes	8.1	−5.3
1996.02.21 12:51	Peru	T	−9.59	−79.59	4	7.4	15	45	7.5	7.3	7.5	101	7.2	Yes	7.3	−6.4
1998.03.25 03:12	Balleny Islands	So	−62.87	149.52	10	7.8	29	75	8.1	7.8	8.1	114	8.0		8.0	−5.4
1998.07.17 08:49	Papua New Guinea	I	−2.96	141.93	7	7.0	15	39	7.0	6.9	6.9	60	7.0		7.0	−6.1
1999.04.08 13:10	Russia−China	D	43.61	130.35	576	7.1	575	12	7.1	7.0	7.0	10	7.1		7.1	−3.6
1999.08.17 00:01	Turkey	S	40.75	29.86	13	7.4	17	22	7.6	7.6	7.7	67	7.4		7.4	−5.6
1999.09.20 17:47	Taiwan	Ro	23.77	120.98	8	7.4	21	34	7.6	7.6	7.8	62	7.6		7.6	−5.3
1999.10.16 09:46	S California	S	34.59	−116.27	20	7.1	15	30	7.1	7.4	7.5	49	7.0		7.0	
2000.06.04 16:28	Sumatra	P	−4.72	102.09	7	7.7	44	41	7.8	7.8	8.1	87	7.9		7.9	−5.3
2000.06.18 14:44	Indian Ocean	So	−13.80	97.45	14	7.5	15	29	7.9	7.8	8.1	39	7.8		7.8	
2000.10.06 04:30	W Honshu	So	35.46	133.13	10	6.5	15	12	6.7	6.8	6.8	53	6.9		6.9	
2000.11.16 04:54	New Ireland	I	−3.98	152.16	33	7.6	24	80	8.0	7.5	7.7	136	7.8	Yes	8.0	−5.7
2000.11.17 21:01	New Britain	I	−5.50	151.78	37	7.4	17	47	7.8	7.5	7.7	76	7.6	Yes	7.7	−5.3
2001.01.26 03:16	S India (Bhuj)	R	23.42	70.23	10	7.6	20	28	7.6	7.8	8.0	31	7.5		7.5	−4.5
2001.02.28 18:54	Washington	P	47.14	−122.72	52	N/A	51	9	6.8	6.6	6.7	8	6.7		6.7	
2001.03.24 06:27	W Honshu	P	34.08	132.53	49	6.7	47	17	6.8	7.0	7.0	25	6.9		6.9	
2001.06.23 20:33	Peru	I	−16.27	−73.64	8	8.3	30	138	8.4	7.5	7.7	156	8.0	Yes	8.4	−5.3
2002.08.19 11:08	Fiji Islands	D	−23.88	178.50	676	7.6	699	21	7.7	7.5	7.7	13	7.6		7.6	−3.1
2002.11.03 22:12	Alaska	RS	63.52	−147.44	4	N/A	15	94	7.9	7.4	7.6	31	7.4		7.4	
2003.01.22 02:06	Mexico	I	18.84	−103.82	24	7.6	26	29	7.5	7.5	7.6	28	7.4	Yes	7.5	−4.3
2003.05.21 18:44	N Algeria	R	36.96	3.63	9	6.7	15	20	6.8	7.0	7.1	23	6.8		6.8	−5.2
2003.07.15 20:27	Carlsberg Ridge	So	−2.56	68.30	10	N/A	15	94	7.5	7.4	7.5	102	7.5		7.5	−6.0
2003.08.04 04:37	Scotia Sea	No	−60.56	−43.49	10	7.1	15	45	7.6	7.3	7.5	45	7.4		7.4	−5.1
2003.09.25 19:50	Hokkaido	I	41.82	143.91	13	8.1	28	64	8.3	7.9	8.2	82	7.9	Yes	8.3	−4.6
2003.09.27 11:33	Siberia	S	50.04	87.81	1	7.3	15	22	7.2	7.4	7.5	77	7.3		7.3	
2003.11.17 06:43	Rat Islands	I	51.15	178.65	5	7.7	22	48	7.7	7.4	7.5	73	7.5	Yes	7.7	−5.3
2003.12.26 01:56	S Iran	S	29.00	58.31	10	6.5	15	11	6.6	6.7	6.7	23	6.6		6.6	
2004.11.11 21:26	Timor	I	−8.17	124.86	10	7.4	17	34	7.5	7.3	7.4	52	7.4	Yes	7.5	−5.1
2004.11.26 02:25	Papua Indonesia	P	−3.57	135.35	10	6.9	12	18	7.1	7.0	7.1	25	7.2		7.2	
2004.11.28 18:32	Hokkaido	I	43.00	145.06	39	7.0	47	10	7.0	7.2	7.3	18	7.1		7.1	−4.3
2004.12.23 14:59	Macquarie	So	−49.31	161.35	35	7.9	28	53	8.1	7.8	8.1	64	7.9		7.9	−4.9
2004.12.26 00:58	Sumatra–Andaman	IT?	3.30	95.98	39	8.2	29	278	9.3	8.1	8.3	418	8.6	Yes	9.2	−5.4

Table 1. (*Continued.*)

Origin time	Event	Type[a]	NEIC Latitude (°)	NEIC Longitude (°)	NEIC Depth (km)	NEIC M_w^{NEIC}	CMT Depth (km)	CMT T_0[b]	CMT M_w^{CMT}	This study M_{wp}	This study M_{wp} Corr[c]	This study, duration–amplitude results T_0 (s)	This study, duration–amplitude results M_{wpd}	This study, duration–amplitude results Moment scaled	This study, duration–amplitude results M_{wpd} scaling	θ^*
2005.02.05 12:23	Celebes Sea	D	5.36	123.21	501	7.0	531	9	7.1	N/A	N/A	15	7.0		7.0	
2005.03.02 10:42	Banda Sea	W	−6.53	129.94	201	7.1	196	9	7.1	7.0	7.1	11	7.1		7.1	
2005.03.28 16:09	N Sumatra	I	2.09	97.11	21	8.1	30	110	8.6	8.2	8.6	108	8.2	Yes	8.6	−4.4
2005.06.13 22:44	Chile	W	−19.99	−69.20	115	7.8	95	13	7.7	7.6	7.8	18	7.7		7.7	
2005.06.15 02:50	N California	So	41.284	−125.983	10	7.1	20	24	7.2	6.9	7.0	34	7.2		7.2	−5.1
2005.07.24 15:42	Nicobar	So	7.92	92.19	16	7.1	12	20	7.2	7.2	7.3	33	7.3		7.3	
2005.08.16 02:46	Honshu	I	38.28	142.04	36	7.0	37	24	7.2	7.4	7.5	54	7.3	Yes	7.3	
2005.09.09 07:26	New Ireland	W	−4.54	153.45	91	7.4	84	58	7.6	7.5	7.7	144	7.7		7.7	−6.3
2005.09.26 01:55	N Peru	W	−5.67	−76.41	127	7.5	108	13	7.5	7.5	7.6	21	7.5		7.5	
2005.10.08 03:50	Pakistan	R	34.54	73.59	26	7.3	12	21	7.6	7.6	7.8	57	7.4		7.4	
2005.11.14 21:38	E Honshu	P	38.10	144.93	11	6.8	18	16	7.0	7.1	7.2	19	7.1		7.1	
2006.01.02 06:10	S Sandwich Islands	So	−60.81	−21.47	10	7.1	20	28	7.4	7.2	7.3	38	7.4		7.4	
2006.01.27 16:58	Banda Sea	D	−5.48	128.09	397	7.5	397	22	7.6	7.5	7.7	21	7.6		7.6	
2006.02.22 22:19	Mozambique	N	−21.32	33.58	11	7.0	12	14	7.0	7.3	7.5	20	7.0		7.0	
2006.04.20 23:25	Koryakia	Ro	61.08	167.09	22	7.3	12	31	7.6	7.3	7.4	38	7.4		7.4	−4.9
2006.05.03 15:26	Tonga	W	−20.13	−174.16	55	7.9	68	47	8.0	7.7	7.9	44	7.9		7.9	−4.3
2006.05.16 10:39	Kermadec	D	−31.78	−179.31	151	7.4	155	26	7.4	7.5	7.6	27	7.5		7.5	
2006.07.17 08:19	Indonesia	T	−9.25	107.41	34	7.2	20	139	7.7	7.2	7.3	178	7.5	Yes	7.7	−6.5
2006.08.20 03:41	Scotia Sea	So	−61.01	−34.39	10	7.0	17	18	7.0	6.9	7.0	17	7.0		7.0	−4.5
2006.09.28 06:22	Samoa Islands	P	−16.57	−172.04	39	6.7	12	11	6.9	7.0	7.1	13	6.9		6.9	−4.3
2006.11.15 11:14	Kuril Islands	I	46.68	153.22	28	7.9	13	106	8.3	7.6	7.7	123	7.9	Yes	8.2	−5.2
2006.12.26 12:26	Taiwan	P	21.83	120.54	10	7.1	23	16	6.9	6.9	7.0	19	7.0		7.0	
2006.12.26 12:34	Taiwan	P	22.01	120.51	10	N/A	34	17	6.8	7.0	7.1	34	7.2		7.2	
2007.01.13 04:23	Kuril Islands	P	46.29	154.45	10	7.9	12	56	8.1	7.8	8.1	88	8.0		8.0	−5.1
2007.01.21 11:27	Molucca Sea	P?	1.24	126.40	22	7.3	22	39	7.5	7.4	7.5	37	7.4		7.4	−4.9
2007.01.30 04:54	Macquarie	So	−54.89	145.73	10	6.8	14	13	6.8	6.7	6.7	17	6.8		6.8	−4.7
2007.04.01 20:39	Solomon Islands	I	−8.45	156.96	10	N/A	23	89	8.1	7.5	7.7	114	7.9	Yes	8.2	−5.1
2007.08.01 17:08	Vanuatu	W	−15.74	167.75	120	7.2	127	19	7.2	7.0	7.0	81	7.4		7.4	−5.9
2007.08.08 17:04	Java	W	−5.97	107.66	289	7.4	304	29	7.5	7.4	7.5	21	7.4		7.4	
2007.08.15 23:40	Peru	I	−13.36	−76.52	30	N/A	33	122	8.0	7.4	7.6	163	7.9	Yes	8.2	−5.6
2007.09.02 01:05	Santa Cruz Islands	I	−11.57	165.81	35	N/A	18	18	7.2	7.0	7.1	72	7.4	Yes	7.5	−5.7
2007.09.10 01:49	Columbia	P	2.95	−78.07	10	N/A	17	18	6.8	6.7	6.8	32	7.0		7.0	
2007.09.12 11:10	Indonesia	I	−4.52	101.38	30	N/A	23	102	8.4	7.7	7.9	131	8.1	Yes	8.5	−4.8
2007.09.12 23:49	Indonesia	WI?	−2.53	100.96	10	N/A	44	71	7.9	7.8	8.0	132	7.9		7.9	−5.8
2007.09.13 03:25	Indonesia	I	−2.22	99.56	10	N/A	12	22	7.0	7.0	7.1	33	7.2	Yes	7.3	−4.9
2007.09.28 13:38	Mariana Islands	D	21.98	142.69	261	7.4	271	13	7.4	7.3	7.4	10	7.3		7.3	−3.3
2007.09.30 05:23	Auckland Islands	Ro	−49.42	163.84	11	N/A	13	35	7.4	7.1	7.2	47	7.4		7.4	
			Mean of $M - M_w^{CMT}$			−0.17			0	−0.17	−0.02		−0.07		0.00	
			Standard deviation of $M - M_w^{CMT}$			0.22			0	−0.27	0.25		0.17		0.11	

2002.11.03 Alaska not used for duration–amplitude regression analysis due to complex nature of source. $M_w^{CMT} = 9.3$ for 2004.12.26 Sumatra–Andaman from Tsai *et al.* (2005).

[a]Earthquake type: I—interplate thrust; T—tsunami earthquake; W—downdip; P—intraplate; D—deep; So—strike-slip oceanic; Ro—reverse-faulting oceanic; No—normal-faulting oceanic; S—strike-slip continental; R—reverse-faulting continental; N—normal-faulting continental.

[b]2 × (CMT centroid time–origin time).

[c]Magnitude-dependent correction of Whitmore *et al.* (2002).

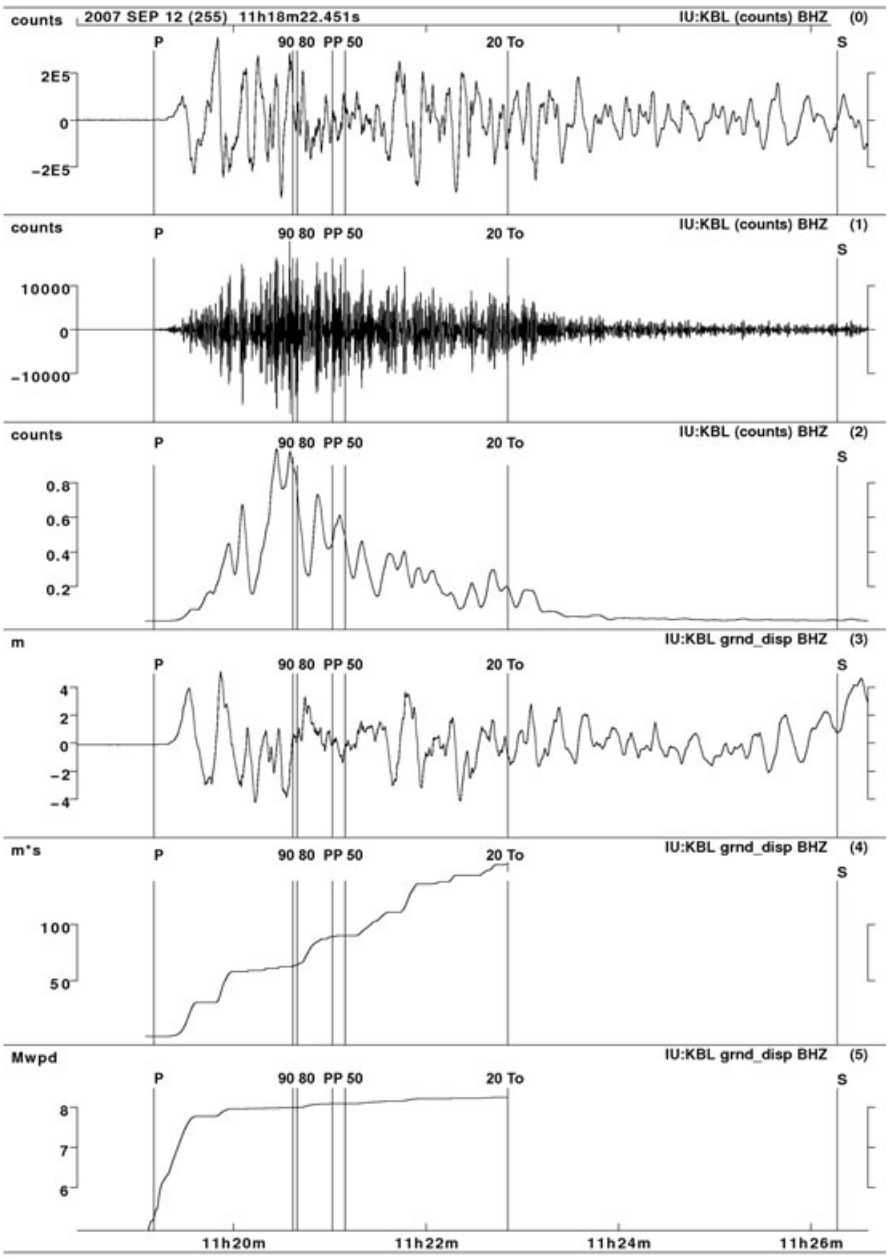

Figure 2. Duration–amplitude processing steps for the 2007 September 12, M8.4 Sumatra earthquake recorded at station IU:KBL at 49° GCD to the northwest of the event. Trace (0): raw, velocity seismogram; trace (1): 1.0 Hz, Gaussian-filtered seismogram; trace (2): smoothed, velocity-squared envelope; trace (3): amplitude corrected, ground-displacement seismogram; trace (4): integral of trace (3) over the source duration using eq. (3) before multiplication by k and C_M, note that for this seismogram the integral over positive values of displacement, $u^+(t)$, in trace (3) gives the maximum result; trace (5): raw M_{pwd} magnitude obtained from trace (3) using eq. (2). *P*, *PP* and *S* indicate the PREM_NC predicted arrival times for the first arriving, *P*, *PP* and *S* waves from the hypocentre. 90, 80, 50 and 20 indicate the times at which the envelope function, trace (2), last drops below 90 (T^{90}), 80 (T^{80}), 50 (T^{50}) and 20 per cent (T^{20}) of its peak value, respectively; To indicates the estimated apparent duration, T_0, for this station. See Appendix B for more details. The *PP* amplitudes on this recording (visible around 11 h 21 m to 11 h 22 m) are larger relative to the *P* amplitudes than they are for most other recordings for this or other events.

the interval T_0 after P of the use in the M_{wp} procedure of the first peak or the first peak-to-peak of the displacement integral (e.g. Tsuboi *et al.* 1999). It is difficult, if not impossible, to justify this procedure theoretically for all event types, event depths and *P*-group phases. However, we find that the use of this procedure, relative to integrating the absolute value of the displacement, gives better agreement with M_w^{CMT} magnitudes, and a value of the constant k in eq. (3) that is closer to the ideal value of 1.

Direct application to large earthquakes

Fig. 3 shows a comparison of the obtained magnitudes, M_{wpd}, with M_w^{CMT} for 79, recent, large earthquakes (M_w^{CMT} 6.6–9.3; Fig. 4 and Table 1) using no knowledge of the event type (Fig. 3a) and using ideal knowledge of the depth, tectonic setting and mechanism for each event (Figs 3b and c). This comparison shows that M_{wpd} matches closely M_w^{CMT} up to M_w^{CMT} ~7.5, but with increasing

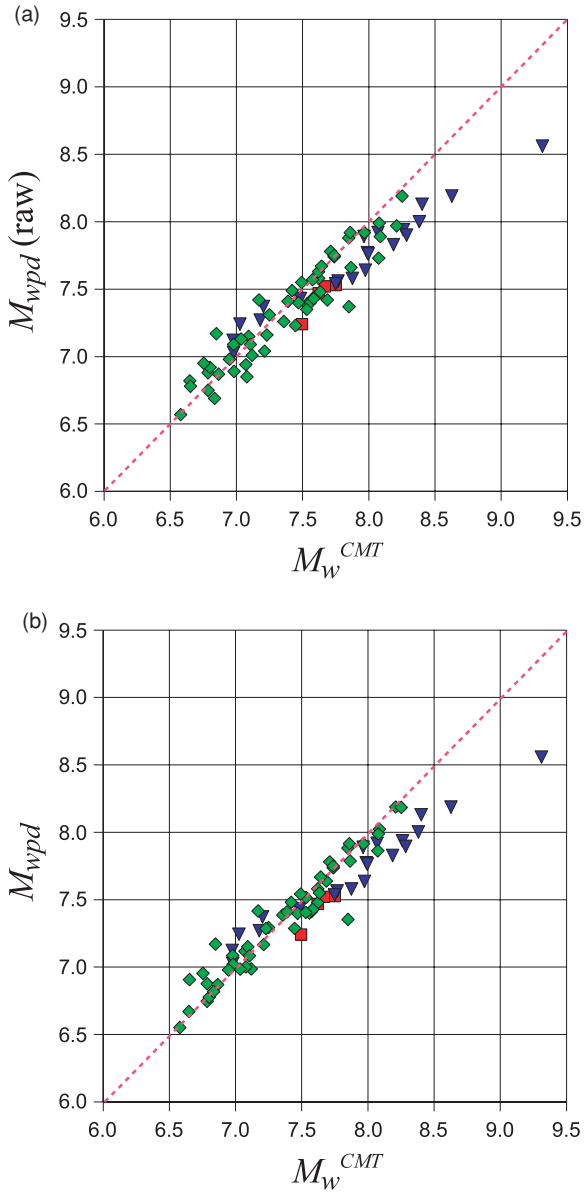

Figure 3. Results for duration–amplitude magnitude M_{wpd} with no moment scaling for interplate thrust or tsunami events (i.e. application of eq. 3) for the studied events (Table 1). (a) 'Raw' M_{wpd} given by direct application of eq. (3) without any corrections for event type compared to CMT magnitude M_w^{CMT}; (b) M_{wpd} (with event type corrections) compared to M_w^{CMT}, (c) $\Delta M = M_{wpd} - M_w^{CMT}$ compared to M_w^{CMT}; ΔM has a standard deviation of $\sigma = 0.17$. Material properties at the source are corrected to correspond to the PREM or PREM_NC model values at the CMT centroid depth (Table 2). The comparison between M_0^{pd} and M_0^{CMT} to determine k in eq. (3) excludes interplate thrust and tsunami events and 2002.11.03 Alaska (labelled RS in plots) which has a poor T_0 estimate due to exceptional source complexity (e.g. Fuis & Wald 2003). Event symbols and labels as in Figs 1 and 4.

magnitude M_{wpd} tends to increasingly underestimate M_w^{CMT}. This is a similar result as obtained for M_{wp} (Fig. 1), though M_{wp} gives an even larger underestimate than M_{wpd} of M_w^{CMT} above $M_w^{CMT} \sim 7.5$, primarily because M_{wp} only considers the first part of the P-wave train while M_{wpd} is based on the full interval of duration T_0 after the P arrival. The NEIC Fast Moment-Tensor magnitude, M_w^{NEIC}, (Sipkin 1994; http://earthquake.usgs.gov), based on waveform inversion, also shows an increasing underestimate of M_w^{CMT} above $M_w^{CMT} \sim 7.5$ (Fig. 1).

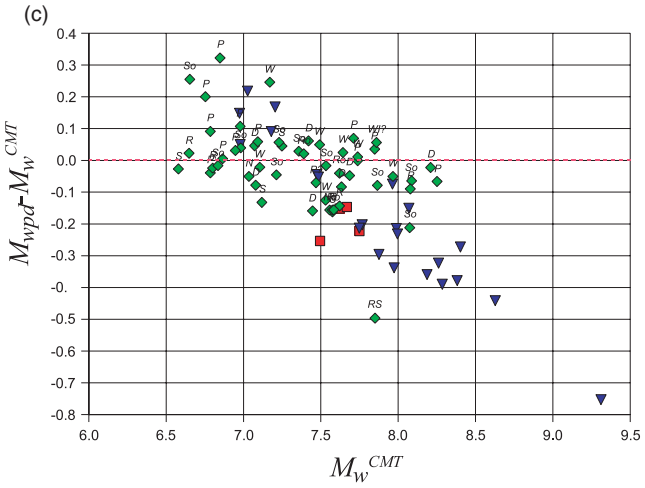

Figure 3. (*continued.*)

Closer examination of Fig. 3 shows that the trend of increasing underestimate of M_w^{CMT} by M_{wpd} (i.e. $\Delta M = M_{wpd} - M_w^{CMT}$ becomes more negative) with increasing M_w^{CMT} occurs mainly for 'interplate thrust' earthquakes (type I in Table 1). M_{wpd} matches well M_w^{CMT} for most events of other types, agreeing over a wide range of magnitudes for strike-slip (types S and So), intraplate (type P), intermediate depth (downdip, type W) and deep earthquakes (type D), and over the limited range of available magnitudes for reverse-faulting (type R and Ro) and normal-faulting (type N and No) crustal earthquakes. It cannot be excluded that tsunami earthquakes (type T) follow a trend similar to that of interplate thrust earthquakes, due to the lack of large tsunami earthquakes.

Thus, we find for larger ($M_w^{CMT} > \sim 7.5$) interplate thrust events that the moments determined from the P-wave train through application of eq. (3), and apparently also through P-waveform inversion (e.g. M_w^{NEIC}, Fig. 1a), underestimate the corresponding CMT moments, derived from inversion of long-period S and surface wave.

Moment scaling for interplate thrust and tsunami earthquakes

The variation of $\Delta M = M_{wpd} - M_w^{CMT}$ differences for interplate thrust earthquakes as a function of M_w^{CMT} (Fig. 3c) and a similar variation as a function of M_{wpd} suggest that more accurate moment estimates for these events, M_0^I, can be obtained by scaling $\hat{M}_0$ with a factor composed of $\hat{M}_0$ raised to some power, that is,

$$M_0^I = \hat{M}_0 \left(\frac{\hat{M}_0}{M_0^{\text{cut-off}}} \right)^R , \qquad (4)$$

where $\hat{M}_0$ is given by eq. (3) and $M_0{}^{\text{cut-off}}$ is a constant cut-off moment below which the scaling is not applied. We also apply the moment scaling, eq. (4), to tsunami earthquakes, since these events fall within the trend of ΔM differences for interplate thrust earthquakes and because it is difficult to distinguish these two types of events in near real-time analysis. Application of the standard moment-magnitude formula, eq. (2), and averaging over stations gives the corresponding P-wave moment magnitude, M_{wpd} (see Appendix B for further details).

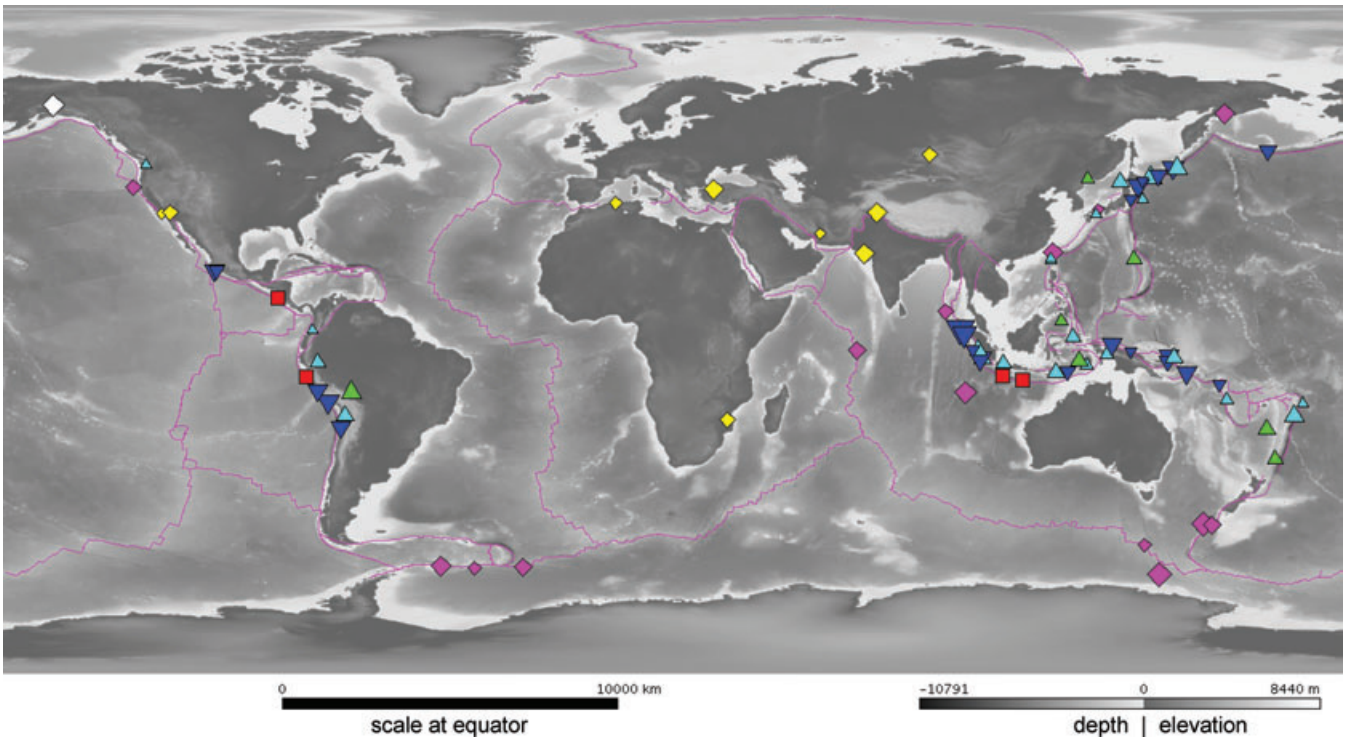

Figure 4. World map showing earthquakes used in this study (*cf.* Table 1). Symbols show earthquake type: I—interplate thrust (blue inverted triangles); T—tsunami earthquake (red squares); W—downdip and P—intraplate (light blue triangles); D—deep (green triangles); So—strike-slip oceanic; Ro—reverse-faulting oceanic and No—normal-faulting oceanic (magenta diamonds); S—strike-slip continental, R—reverse-faulting continental and N—normal-faulting continental (yellow diamonds); hybrid events (white diamonds). Symbol size is proportional to event magnitude. Base map from NGDC (2006); plate boundaries (magenta lines) from Coffin *et al.* (1998).

Application with moment scaling to large earthquakes

Application of eq. (4) to the interplate thrust and tsunami events from the set of studied earthquakes over a range of values of R and $M_0^{\text{cut-off}}$ gives $P \approx 0.45$ and $M_0^{\text{cut-off}} \approx 7.5 \times 10^{19}$ N - m (equivalent to $M_w \approx 7.2$) for the best match of M_{wpd} to M_w^{CMT} (The optimal values of $M_0^{\text{cut-off}}$ and R are sensitive to the algorithms used to estimate T_0 and moment, see Appendix B). Thus, we arrive at a preferred, duration–amplitude expression for moment estimation,

$$M_0^{pd} = \hat{M}_0 \left(\frac{\hat{M}_0}{M_0^{\text{cut-off}}} \right)^{0.45}, \tag{5a}$$

for interplate thrust and tsunami events with $\hat{M}_0 \geq M_0^{\text{cut-off}}$, and

$$M_0^{pd} = \hat{M}_0, \tag{5b}$$

otherwise, where $\hat{M}_0$ is given by eq. (3) with $C_M = 1.62 \times 10^{19}$ and $k \approx 1.2$ (see Appendices A and B; see Table 2 for depth corrections). M_{wpd} magnitudes determined using eqs (5a), (5b) and (2) for the studied earthquakes are shown in Fig. 5 and Table 1. These results show that M_{wpd}, with moment scaling for interplate thrust and tsunami events, matches M_w^{CMT} typically within ± 0.2 magnitude units, with a standard deviation of only $\sigma = 0.11$.

Estimation of energy-to-moment parameter Θ^*

The energy-to-moment parameter, Θ, (e.g. Newman & Okal 1998; Weinstein & Okal 2005) for identification of tsunami earthquakes is defined as

$$\Theta = \log_{10} \frac{E}{M_0}, \tag{6}$$

where E is the radiated seismic energy and M_0 the moment. Weinstein & Okal (2005) note that standard earthquake scaling laws (assuming a constant stress drop) predict a value of $\Theta \approx -4.9$, but find Θ values around -6.0 or less for tsunami earthquakes. Thus, anomalously low values of a rapid estimate of Θ, combined with knowledge of an earthquake's location, size, tectonic setting and likely source type, can be an important indicator of a potential tsunami earthquake.

From duration–amplitude estimates of moment, M_0^{pd}, and duration, T_0, we can obtain an approximation to Θ, Θ^*, through

Table 2. Magnitude corrections for event depth (PREM/PREM_NC).

Depth range (km)	Correction (magnitude units)
<15 continental crust	−0.28 (not used in this study)
<24.4 continental crust	−0.15
<24.4 other types	No correction
24.4–220	No correction
220–271	+0.05
271–371	+0.06
371–400	+0.07
400–471	+0.12
471–571	+0.15
571–671	+0.18
≥671	+0.22

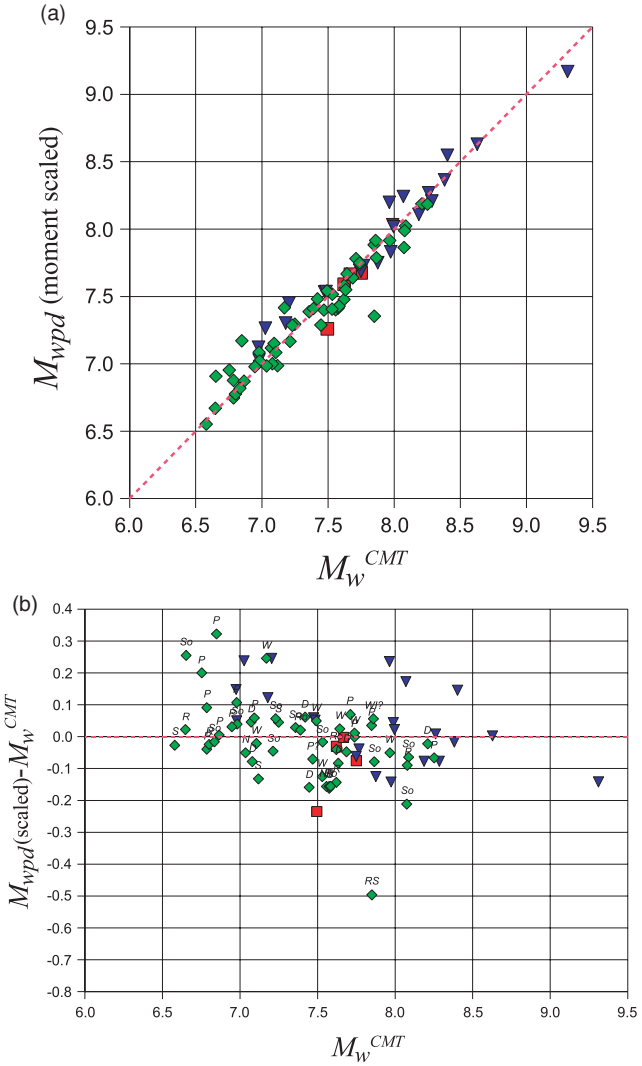

Figure 5. Results for duration–amplitude magnitude M_{wpd} corrected with moment scaling for interplate thrust and tsunami events (i.e. application of eqs 3 and 5a or 5b) for the studied events (Table 1). (a) M_{wpd} compared to CMT magnitude $M_{\rm w}^{\rm CMT}$; (b) $\Delta M = M_{wpd} - M_{\rm w}^{\rm CMT}$ compared to $M_{\rm w}^{\rm CMT}$. ΔM has a standard deviation of $\sigma = 0.11$. Material properties at the source are corrected to correspond to the PREM or PREM_NC model values at the CMT centroid depth (Table 2). Event symbols and labels as in Figs 1 and 4.

application of the energy–duration relation of Lomax *et al.* (2007),

$$M_0^{ED} = cE^{1/2}T_0^{3/2}, \tag{7}$$

where $c \approx 1.55 \times 10^{10}$ for average crust–upper-mantle material properties. Substituting M_0^{pd} for M_0^{ED} in eq. 7, solving for E and substituting into eq. 6, gives,

$$\Theta^* = \log_{10}\left(c^{-2}M_0^{pd}/T_0^3\right). \tag{8}$$

The approximate Θ^* values should only be used when the uncertainty σ_{T_0} in T_0 is small, since the dependence of Θ^* on T_0^{-3} amplifies error in T_0 into Θ^*. Θ^* values determined using eq. (8) for the studied earthquakes where $\sigma_{T_0} < 2T_0/3$ are listed in Table 1 and plotted in Fig. 6 as function of M_{wpd}.

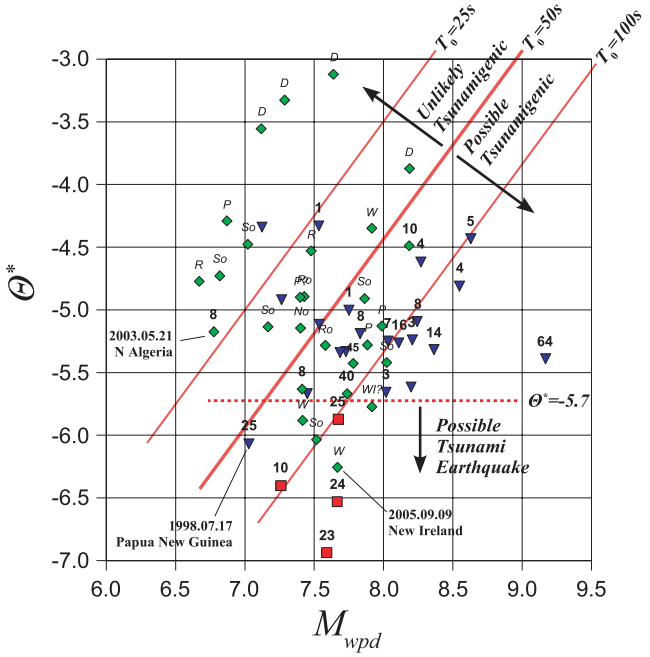

Figure 6. Θ^* values from application of eq. (8) to duration–amplitude results with moment scaling for interplate thrust and tsunami events (i.e. application of eqs 3 and 5A or 5B) for the studied events where $\sigma_{T_0} < 2T_0/3$ or $I_{\rm t} \geq 1$ (Table 1). Θ^* values are plotted against M_{wpd}. Bold numbers show the measure of tsunami importance, $I_{\rm t}$, based on maximum water height and descriptive indices of tsunami effects from the NOAA/WDC Historical Tsunami Database (NGDC 2008). Event symbols as in Fig. 1 and event type labels (shown for events with $I_{\rm t} < 1$) as in Fig. 4 and Table 1. Dashed red line shows $\Theta^* = -5.7$ cut-off for identification of tsunami earthquakes; lines of constant T_0 are shown in red; thick red line shows $T_0 = 50$ s cut-off for identification of tsunamigenic earthquakes.

PRACTICAL APPLICATION OF THE DURATION–AMPLITUDE PROCEDURE

Without moment scaling (eq. 5a) M_{wpd} provides a closer match to $M_{\rm w}^{\rm CMT}$ magnitude, including for larger interplate thrust events and tsunami earthquakes, than do other procedures for rapid magnitude estimation (standard deviation of $\sigma = 0.17$; *cf.* Figs 1, 3b and c, Table 1). Furthermore, a 'raw' M_{wpd} given by direct application of eq. (3) without any corrections for event type (e.g. no crustal correction for shallow continental events, no correction for radiation pattern for strike-slip events) still matches $M_{\rm w}^{\rm CMT}$ with $\sigma = 0.18$ (Fig. 3a). However, as with all rapid analysis methodologies based on body wave signals, knowledge of the hypocentre location, the tectonic setting and likely focal mechanism is needed to obtain the best and most informative results.

Rapid identification of event type and other source parameters

Obtaining the best match of M_{wpd} to $M_{\rm w}^{\rm CMT}$ requires identification of interplate thrust and tsunami earthquakes for application of the moment scaling, and a reliable depth estimate and further classification by type, for example, as continental, oceanic, strike-slip, or deep, for application of corrections for PREM properties at the source depth (Table 2). The correction for PREM properties at the source depth relative to average, upper-mantle properties is only significant (i.e. gives a magnitude change $\delta M > 0.1$) for events deeper than 400 km and for continental crustal events. Also, the corrections for

continental crustal type ($\delta M \approx -0.15$) and for strike-slip mechanism ($\delta M \approx 0.13$) approximately cancel for continental, strike-slip events. However, not all events can be easily classified within minutes after OT. For example, we classify the 2007 September 12, 23:49, M7.9 Indonesia earthquake as a downdip event (based on the epicentral location and the CMT centroid depth of 44 km; Table 1) giving $M_{wpd} = 7.9$; but the epicentral location and shallow initial depth estimate for this event could imply that it is an interplate thrust event, in which case the amplitude–duration moment scaling should be applied, giving $M_{wpd} = 8.2$.

In the near future, information on the hypocentre location, tectonic setting and likely focal mechanism of an event should be available before the duration–amplitude analysis is performed, thus likely interplate thrust and tsunami events, the event type and the approximate source depth can be identified rapidly. Currently, the epicentre for most events can be determined accurately within minutes of OT; the main difficulties lie with the determination of the hypocentral depth and, secondarily, of the source mechanism. Improvements in depth determination based on standard earthquake location procedures are not likely, due to fundamental limitations of the ray coverage at the source of the rapidly available, first P-arrival data. Instead, improved depth estimation may come from prior information on the depth of seismicity and plate boundaries (e.g. Hayes & Wald 2008) which can provide a likelihood function for depth based on the epicentral location. Similarly, maps of crustal types (e.g. Mooney *et al.* 1998; Bassin *et al.* 2000) can provide a likelihood function for tectonic setting based on the epicentral location. For the determination of M_{wpd} knowledge of the source mechanism, though less important than event depth, could provide further constraint on the tectonic setting and event type (e.g. distinguishing between interplate thrust and normal-faulting, outer-rise earthquakes, both of which occur near subduction zones). Rapid and robust estimation of mechanism may be possible using existing procedures based on the first-motions and initial amplitudes of P waveforms.

DISCUSSION

We have introduced a duration–amplitude procedure to obtain rapidly an earthquake moment, M_0^{pd}, and moment magnitude, M_{wpd}, from P-wave recordings at teleseismic distances. Because the required recordings are available in near real time at earthquake and tsunami monitoring centres, M_{wpd} can be available within about 20 min after OT. For major and great earthquakes ($M_{\rm w}^{\rm CMT} \geq 7.0$), M_{wpd} (with moment scaling for interplate thrust and tsunami events) matches $M_{\rm w}^{\rm CMT}$ typically within ± 0.2 magnitude units, with a standard deviation of only $\sigma = 0.11$ (Fig. 5, Table 1). In addition, M_{wpd} does not exhibit saturation; that is, for the largest events, M_{wpd} does not systematically underestimate $M_{\rm w}^{\rm CMT}$ and $\Delta M = M_{wpd} - M_{\rm w}^{\rm CMT}$ remains small. Thus, M_{wpd} equals or outperforms other procedures for rapid moment-magnitude determination. The results of other procedures, using different and smaller sets of events than used here, are

(1) $M_{\rm ED}$ (Lomax *et al.* 2007) matches $M_{\rm w}^{\rm CMT}$ typically within ± 0.3 magnitude units, with $\sigma = 0.16$, and $\Delta M = M^{\rm est} - M_{\rm w}^{\rm CMT}$ for $M_{\rm ED}$ does not change with increasing $M_{\rm w}^{\rm CMT}$;

(2) $m_{\rm Bc}$ (Bormann et al. 2006; Bormann & Saul 2008) matches $M_{\rm w}^{\rm CMT}$ typically within ± 0.5 magnitude units, with $\sigma = 0.26$, but there is a trend in ΔM for uncorrected $m_{\rm Bc}$ to become more positive with decreasing $M_{\rm w}^{\rm CMT}$ (the large σ with respect to $M_{\rm w}^{\rm CMT}$ is expected since $m_{\rm Bc}$ is fundamentally an energy magnitude, while the trend in ΔM can be compensated via a regression relation given by Bormann & Saul 2008);

(3) the rapid magnitude estimates of Hara (2007) shows a match with $M_{\rm w}^{\rm CMT}$ typically within ± 0.3 magnitude units, with $\sigma = 0.18$, and ΔM for this magnitude is stable or possibly becomes more negative with increasing $M_{\rm w}^{\rm CMT}$;

(4) our corrected M_{wp} results (Fig. 1c; Table 1) match $M_{\rm w}^{\rm CMT}$ typically within ± 0.5 magnitude units, with $\sigma = 0.25$, and ΔM for M_{wp} becomes rapidly increasingly negative with increasing $M_{\rm w}^{\rm CMT}$.

The improved agreement between M_{wpd} and $M_{\rm w}^{\rm CMT}$ relative to other rapid procedures, including M_{wp}, can be attributed primarily to the use in eq. (3) of the full t_P to $t_P + T_0$ interval for integration with testing of integrals over positive and negative values of displacement, and to the application of the moment scaling, eq. (5a), for interplate thrust and tsunami earthquakes. This agreement is also dependent on the use of additional corrections for certain events types, and a robust procedure for estimating T_0 from high-frequency seismograms (see Appendices A and B for details). Indeed, much of the scatter in M_{wpd} versus $M_{\rm w}^{\rm CMT}$ for $M_{\rm w} < \sim 7.2$ (Figs 3 and 5) can be attributed to large errors in the T_0 estimation. The M_{wpd} results indicate that testing of the integral in eq. (3) over positive and negative values of displacement separates adequately the direct P waves from surface reflection phases and other secondary phases, even when the rupture duration, T_0, is large. This testing is analogous to the selection in the M_{wp} magnitude procedure of the larger of the first peak or the first peak-to-peak amplitude of the integral eq. (1). The moment scaling used here is likely related to the magnitude-dependent correction to M_{wp} proposed by Whitmore *et al.* (2002) and to the values of the coefficients in the regression of Hara (2007), in both cases applied to all earthquakes. In contrast, we find here that moment scaling is only needed for interplate thrust earthquakes, and possibly for tsunami earthquakes. The characteristics of the duration–amplitude procedure noted above show that it is an extension of the M_{wp} moment-magnitude algorithm, recalling also that both procedures are ultimately based on eq. (1).

Energy-to-moment parameter Θ^* and tsunamigenic potential

We have shown that the duration–amplitude estimates of moment, M_0^{pd}, and duration, T_0, can be combined with the energy–duration relation of Lomax *et al*. (2007) to provide a rapid approximation, Θ^*, (eq. 8) to the energy-to-moment parameter Θ used for identification of tsunami earthquakes (e.g. Newman & Okal 1998; Weinstein & Okal 2005). Duration–amplitude estimates of Θ^* using eq. (8) are listed in Table 1 and are shown in Fig. 6. To simulate the results that would be available with rapid application of the duration–amplitude procedure, we show Θ^* values only for events where $\sigma_{T_0} < 2T_0/3$ (a stronger cut-off would be used in practice) and we plot Θ^* against M_{wpd} and not $M_{\rm w}^{\rm CMT}$, which is not available rapidly.

The duration–amplitude estimates of Θ^* are $\Theta^* \leq -5.8$ for all studied tsunami earthquakes, thus $\Theta^* \leq -5.7$ may be an appropriate cut-off for identification of these events (Fig. 6). Some interplate thrust, downdip and strike-slip events have low Θ^* values ($\Theta^* \leq -5.5$), and deep events have high Θ^* values. Θ^* is low, $\Theta^* = -6.1$, for a tsunamigenic, interplate thrust event (1998.07.17 Papua New Guinea) that is considered not to be a tsunami earthquake (Heinrich *et al.* 2001; Okal 2003). Low values of Θ^* for strike-slip earthquakes can be attributed to overestimate of T_0 for smaller events, perhaps related to the strike-slip radiation pattern producing anomalously low amplitudes and an excessively long coda in the high-frequency

seismograms used to estimate T_0. Weinstein & Okal (2005) also find anomalously low values of Θ for several strike-slip events. Similarly, the low value $\Theta^* = -6.3$ for a downdip earthquake (W; 2005.09.09 New Ireland) can be attributed to overestimate of T_0 for this event due to anomalously high-frequency signal in the depth phases *pP* and *sP*.

We include in Fig. 6 an approximate measure of tsunami importance, I_t, based on maximum water height in metres, h, and 0–4 descriptive indices, i, of tsunami effects (deaths, injuries, damage, houses destroyed) from the NOAA/WDC Historical Tsunami Database (NGDC 2008),

$$I_t = h + i_{\text{deaths}} + i_{\text{injuries}} + i_{\text{damage}} + i_{\text{houses destroyed}}. \quad (9)$$

For completeness, two events with $\sigma_{T_0} > 2T_0/3$ but which have $I_t \geq 1$ are also indicated in Fig. 6 (1999.08.17, M_w7.6, Turkey, $I_t = 8$; 2003.01.22, M_w7.5, Mexico, $I_t = 1$). Strikingly, Fig. 6 shows no clear relationship between I_t and Θ^*, indicating that Θ, while a robust indicator for tsunami earthquakes, is not a good indicator for tsunamigenic potential in general. Similarly, there is no clear relationship between I_t and M_w, as represented by M_{wpd}. Instead, we find that the majority of tsunamigenic events fall to one side of diagonal lines of constant T_0, as defined by eq. (8). A good separation between events with $I_t < 1$ (unlikely tsunamigenic events) and those with $I_t > 1$ (possible tsunamigenic events) is given by the line $T_0 = 50$ s. The only major exception is 2003.05.21, M_w6.8, N Algeria, a submarine, shallow, thrust event that produced larger than expected tsunami waves, perhaps due to focusing of tsunami waves or slope failure near the source (Hébert & Alasset 2003). These results suggest that a value of $T_0 \geq 50$ s obtained with the rapid, duration–amplitude procedure, if the uncertainty in T_0 is low, is a reliable indicator of a possible destructive, tsunamigenic event.

The importance of the T_0 estimate for the determination of the tsunamigenic potential of an earthquake, and to a lesser degree for the determination of M_{wpd}, combined with the large uncertainties in T_0 obtained for smaller events and certain event types, indicates a need for future work on improving the accuracy and robustness of the T_0 determination.

Application at local and regional distances

The duration–amplitude methodology may be applicable at local and regional distances, that is, GCD $< 30^\circ$, thus reducing the time delay after OT for obtaining size estimates for larger events. However, relative to the teleseismic analysis presented in this paper, there are many complications when working at local and regional distances. The main difficulty is that significant *S* signal may remain on the high-frequency, *P*-wave seismograms used for determination of the duration, T_0, which complicates the analysis of larger and longer duration events. In this case, the direct *P*-wave radiation can often be isolated by applying the narrow-band, Gaussian filtering at higher frequencies (e.g. 5–20 Hz), but this requires that high dynamic-range, high sample-rate data are available. At regional distances, there may be additional difficulties due to the multitude of direct, reflected, refracted and converted *P*- and *S*-wave types that can contribute to the *P*-wave train.

Physical implications of moment scaling

The increasing underestimate of M_w^{CMT} with increasing magnitude by unscaled M_{wpd} for interplate thrust (and possibly tsunami) earthquakes (Fig. 3) and the consequent need for moment scaling (eq. 5a) may have important physical implications. The increasing underestimate of M_w^{CMT} is probably not due to station site or path effects, since then it would occur for all event types, and it is probably not a direct effect of the source mechanism radiation pattern, since then it would not vary with event size. In addition, examination of M_{wpd} estimates obtained with different long-period cut-offs (Appendix C) indicates that the increasing underestimate of M_w^{CMT} is not due to magnitude saturation due to insufficient, long-period signal. Thus, the increasing underestimate of M_w^{CMT} may be associated with near-source, dynamic phenomena unique to larger interplate thrust (and possibly tsunami) earthquakes, events which occur at shallow depths. The form of the moment scaling, eq. (5a), suggests a deficiency that increases with event size in the amplitude of far-field, radiated *P* waves relative to the amplitudes expected from the CMT results.

The destructive interference of *pP* or *sP* waves with direct, downgoing *P* waves is an often cited explanation for reduced, far-field *P* amplitudes. This is, however, a kinematic mechanism which, for large, shallow earthquakes, must be cast into a dynamic framework where the interference will occur within the rupture volume and simultaneous with rupture. The deficiency in amplitude may therefore be associated with a near-field mechanism which reduces the radiated kinetic energy while maintaining the seismic energy balance. A candidate mechanism would be excessive dissipation of the strain energy released during faulting by gravitational, fracturing and frictional processes on or near the fault, alimented by complex wave interactions around the rupturing fault. Such interactions could involve waves reflected, generated or trapped near the free surface, such as the near-field analogues of *pP* and *sP*, which may interfere destructively with the fault displacements that produce far-field *P* waves, reducing the amplitude of these waves. We can then hypothesizes a transfer of kinetic energy along strike and in the direction of rupture (for long thrust faults) by waves from earlier rupture, producing dynamic stress loading across the fault around the rupture front and augmenting the loading due to nearby fault displacements.

Such dynamic loading near the rupture front could raise the shear stress above the failure yield stress (e.g. Scholz 2002), decrease the normal stress and thus decrease the effective yield stress (e.g. Oglesby *et al.* 2000), or drive rupture in zones with a velocity-strengthening friction behaviour (e.g. Scholz 1998). In all these cases, increased fracture, rupture and slip would be induced at the rupture front, including on parts of the fault for which the initial shear stress was much less than the static yield stress, or which have velocity-strengthening behaviour, likely in the shallower, updip parts of subduction thrusts (e.g. Scholz 1998). Thus, the moment scaling could be a manifestation of a 'self-driving' mechanism for large interplate thrust (and possibly tsunami) earthquakes in which an anomalously large proportion of the energy released during rupture is re-absorbed locally to further drive the rupture, and thus to make the earthquake large.

CONCLUSIONS

We have presented a duration–amplitude procedure for determination of a moment magnitude, M_{wpd}, for large earthquakes within 20 min of the event OT using teleseismic *P*-wave recordings. We find that a scaling of the moment estimates for interplate thrust and possibly tsunami earthquakes is necessary to best match M_w^{CMT}. With this scaling, M_{wpd} equals or outperforms other approaches to rapid magnitude determination, and does not exhibit saturation.

The characteristics of the duration–amplitude methodology make it an extension of the widely used, M_{wp}, rapid magnitude procedure. The need for a moment scaling for interplate thrust and possibly tsunami earthquakes may have important implications for the source physics of these events.

As with other rapid, earthquake-analysis procedures, obtaining the best match of M_{wpd} to $M_{\mathrm{w}}^{\mathrm{CMT}}$ requires identification of the event type, a reliable depth estimate, and other source parameters. Many groups are currently working on providing this information more reliably and more rapidly.

The duration–amplitude procedure allows rapid estimation of an energy-to-moment parameter Θ^* used for identification of tsunami earthquakes. However, our results show that neither Θ^* nor M_{w} is a good indicator for tsunamigenic events in general. For these events, we find that a reliable indicator is simply that the duration–amplitude duration, T_0, is greater than about 50 s.

ACKNOWLEDGMENTS

This work benefited greatly from discussions with Peter Bormann, Massimo Cocco, Paul Earle, Goran Ekström, Barry Hirshorn, Chris Marone, Stefan Nielsen and Martin Vallée, and from thorough reviews by two anonymous reviewers. The work of A.L. was supported by personal funds; A.M. has been supported by the INGV-DPC (Dipartimento della Protezione Civile) S4 project—''Stima dello scuotimento in tempo reale e quasi-reale per terremoti significativi in territorio nazionale''. We use the Java programme SeisGram2K (http://www.alomax.net/software) for seismogram analysis, processing and figures, and OpenOffice.org Calc for graphs. The IRIS DMC (http://www.iris.edu) provided access to waveforms used in this study.

REFERENCES

Aki, K. & Richards, P.G., 1980. *Quantitative Seismology: Theory and Practice,* W. H. Freeman, New York, 948 pp.

Bassin, C., Laske, G. & Masters, G., 2000. The current limits of resolution for surface wave tomography in North America, *Eos, Trans. Am. geophys. Un.,* **81,** 897.

Boatwright, J. & Choy, G.L., 1986. Teleseismic estimates of the energy radiated by shallow earthquakes, *J. geophys. Res.,* **91,** 2095–2112.

Bormann, P. (ed.), 2002. *IASPEI New Manual of Seismological Observatory Practice (NMSOP),* Vols. 1 and 2, GeoForschungsZentrum, Potsdam, 1250 pp.

Bormann, P. & Saul, J., 2008. Earthquake magnitude, in *Encyclopedia of Complexity and Systems Science,* ed. Meyers, A., Springer, Berlin, in press.

Bormann, P. & Wylegalla, K., 2005. Quick estimator of the size of great earthquakes, *Eos, Trans. Am. geophys. Un.,* **86**(46), 464.

Bormann, P., Wylegalla, K. & Saul, J., 2006. Broadband body-wave magnitudes mB and mBc for quick reliable estimation of the size of great earthquakes, in *USGS Tsunami Sources Workshop 2006*, poster, available at: http://spring.msi.umn.edu/USGS/Posters/Bormann_etal_poster.pdf.

Choy, G.L. & Boatwright, J.L., 1995. Global patterns of radiated seismic energy and apparent stress, *J. geophys. Res.,* **100,** 18 205–18 228.

Coffin, M.F., Gahagan, L.M. & Lawver, L.A., 1998. Present-day Plate Boundary Digital Data Compilation, Technical Report No. 174, Institute for Geophysics, University of Texas, 5 pp.

Dziewonski, A.M. & Anderson, D.L., 1981. Preliminary Reference Earth Model (PREM), *Phys. Earth Planet. Inter.,* **25,** 297–356.

Dziewonski, A., Chou, T.A. & Woodhouse, J.H., 1981. Determination of earthquake source parameters from waveform data for studies of global and regional seismicity, *J. geophys. Res.,* **86,** 2825–2852.

Ekström, G., 1994. Rapid earthquake analysis utilizes the internet, *Comp. Phys.,* **8,** 632–638.

Fuis, G.S. & Wald, L.A., 2003. Rupture in South-Central Alaska—the Denali Fault earthquake of 2002, Fact Sheet 014-03, U.S.G.S.

Granville, J.P., Richards, P.G., Kim W.-Y. & Sykes, L.R., 2005. Understanding the differences between three teleseismic mb Scales, *Bull. seism. Soc. Am.,* **95,** 1809–1824, doi:10.1785/0120040159.

Hanks, T. & Kanamori, H., 1979. A moment magnitude scale, *J. geophys. Res.,* **84,** 2348–2350.

Hara, T., 2007. Measurement of the duration of high-frequency energy radiation and its application to determination of the magnitudes of large shallow earthquakes, *Earth Planets Space,* **59,** 227–231.

Hayes, G.P. & Wald, D.J., 2008. Developing framework for constraining the geometry of the seismic rupture plane—a probabilistic approach, *Seis. Res. Lett.,* **79,** 344–344.

Hébert, H. & Alasset, P.-J., 2003. The tsunami triggered by the 21 May 2003 Algiers earthquake, *CSEM-EMSC Newslett.,* **20,** 10–12.

Heinrich, P., Piatanesi, A. & Hebert, H., 2001. Numerical modelling of tsunami generation and propagation from submarine slumps: the 1998 Papua New Guinea event, *Geophys. J. Int.,* **145,** 97–111.

Hirshorn, B., 2006. Hagemeyer, R.H. Pacific Tsunami Warning Center, presentation for PTWS-WG1, Intergovernmental Coordination Group for the Pacific Tsunami Warning and Mitigation System (ICG/PTWS), Melbourne, Australia, available at: http://ioc3.unesco.org/ptws.

Lay, T., 2002. The Earth's Interior, in *International Handbook of Earthquake and Engineering Seismology,* pp. 829–860, eds Lee, W.H.K., Kanamori, H., Jennings, P.C. & Kisslinger, C., Academic Press, Amsterdam.

Lockwood, O.G. & Kanamori, H., 2006. Wavelet analysis of the seismograms of the 2004 Sumatra-Andaman earthquake and its application to tsunami early warning, *Geochem. Geophys. Geosyst.,* **7,** Q09013, doi:10.1029/2006GC001272.

Lomax, A., 2005. Rapid estimation of rupture extent for large earthquakes: application to the 2004, M9 Sumatra-Andaman mega-thrust, *Geophys. Res. Lett.,* **32,** L10314, doi:10.1029/2005GL022437.

Lomax, A. & Michelini, A., 2005. Rapid determination of earthquake size for Hazard warning, *Eos, Trans. Am. geophys. Un.,* **86**(21), 202.

Lomax, A., Michelini, A. & Piatanesi, A., 2007. An energy-duration procedure for rapid determination of earthquake magnitude and tsunamigenic potential, *Geophys. J. Int.,* **170,** 1195–1209, doi:10.1111/j.1365-246X.2007.03469.x

Kanamori, H., 1972. Mechanism of tsunami earthquakes, *Phys. Earth Planet. Int.,* **6,** 346–359.

Kanamori, H. & Rivera, L., 2004. Static and dynamic scaling relations for earthquakes and their implications for rupture speed and stress drop, *Bull. seism. Soc. Am.,* **94,** 314–319.

Kawakatsu, H., 1995. Automated near-realtime CMT inversion, *Geophys. Res. Lett.,* **22,** 2569–2572.

Kerr, R.A., 2005. Failure to gauge the quake crippled the warning effort, *Science,* **307,** 201.

Menke, W. & Levin, V., 2005. A strategy to rapidly determine the magnitude of great earthquakes, *Eos, Trans. Am. geophys. Un.,* **86**(19), 185, doi:10.1029/2005EO190002.

Mooney, W., Laske, G. & Masters, G., 1998. Crust 5.1: a global crustal model at 5×5 degrees, *J. geophys. Res.,* **103,** 727–747.

NGDC, 2006. ETOPO2v2, 2-minute Gridded Global Relief Data, U.S. Department of Commerce, National Oceanic and Atmospheric Administration, National Geophysical Data Center.

NGDC, 2008. NOAA/WDC Historical Tsunami Database: Tsunami source event search, available at: http://www.ngdc.noaa.gov/seg/hazard/tsu_db.shtml

Newman, A.V. & Okal, E.A., 1998. Teleseismic estimates of radiated seismic energy: the E/M_0 discriminant for tsunami earthquakes, *J. geophys. Res.,* **103**(11), 26 885–26 898.

Oglesby, D.D., Archuleta, R.J. & Nielsen, S.B., 2000. The three-dimensional dynamics of dipping faults, *Bull. seism. Soc. Am.,* **90,** 616–628.

Okal, E.A., 2003. T Waves from the 1998 Papua New Guinea earthquake and its aftershocks: timing the tsunamigenic slump, *Pure Appl. Geophys.,* **160,** 1843–1863.

Okal, E.A. & Talandier, J., 1989. Mm: a variable period mantle magnitude, *J. geophys. Res.,* **94,** 4169–4193.
Polet, J. & Kanamori, H., 2000. Shallow subduction zone earthquakes and their tsunamigenic potential, *Geophys. J. Int.,* **142,** 684–782.
PTWC, 2006a. Tsunami Bulletin Number 001, issued at 0836Z 17 Jul 2006, Pacific Tsunami Warning Center/NOAA/NWS.
PTWC, 2006b. Tsunami Bulletin Number 002, issued at 1108Z 17 Jul 2006, Pacific Tsunami Warning Center/NOAA/NWS.
Satake, K., 2002. Tsunamis, in *International Handbook of Earthquake and Engineering Seismology,* pp. 437–451, eds Lee, W.H.K., Kanamori, H., Jennings, P.C. & Kisslinger, C., Academic Press, Amsterdam.
Scholz, C.H., 1998. Earthquakes and friction laws, *Nature,* **391,** 37–42.
Scholz, C.H., 2002. *The Mechanics of Earthquakes and Faulting,* 471 pp., Cambridge University Press, New York.
Shearer, P., 1999. *Introduction to Seismology,* 260 pp., Cambridge University Press, New York.
Sipkin, S.A., 1994. Rapid determination of global moment-tensor solutions, *Geophys. Res. Lett.,* **21,** 1667–1670.
Stein, S. & Okal, E.A., 2007. Ultralong period seismic study of the December 2004 Indian Ocean earthquake and implications for regional tectonics and the subduction process, *Bull. seism. Soc. Am.,* **97,** S279–S295; doi:10.1785/0120050617.
Tsai, V.C., Nettles, M., Ekström, G. & Dziewonski, A.M., 2005. Multiple CMT source analysis of the 2004 Sumatra earthquake, *Geophys. Res. Lett.,* **32,** L17304, doi:10.1029/2005GL023813.
Tsuboi, S., 2000. Application of M_{wp} to tsunami earthquake, *Geophys. Res. Lett.,* **27,** 3105–3108.
Tsuboi, S., Abe, K., Takano, K. & Yamanaka, Y., 1995. Rapid determination of *Mw* from broadband P waveforms, *Bull. seism. Soc. Am.,* **85,** 606–613.
Tsuboi, S., Whitmore, P.M. & Sokolowski, T.J., 1999. Application of M_{wp} to deep and teleseismic earthquakes, *Bull. seism. Soc. Am.,* **89,** 1345–1351.
UNESCO, 2005. International Coordination Meeting for the Development of a Tsunami Warning and Mitigation System for the Indian Ocean within a Global Framework, IOC Workshop Report 196, 103 pp.
Vassiliou, M.S. & Kanamori, H., 1982. The energy release in earthquakes, *Bull. seism. Soc. Am.,* **72,** 371–387.
Weinstein, S.A. & Okal, E.A., 2005. The mantle wave magnitude M_m and the slowness parameter *THETA*: five years of real-time use in the context of tsunami warning, *Bull. seism. Soc. Am.,* **95,** 779–799.
Whitmore, P.M., Sokolowski, T.J., Tsuboi, S. & Hirshom, B., 2002. Magnitude-dependent correction for MWP, *Sci. Tsunami Hazards,* **20**(4), 187–192.

APPENDIX A: FAR-FIELD ESTIMATION OF SEISMIC MOMENT FROM *P* WAVEFORMS

Following Aki & Richards (1980), Boatwright & Choy (1986), Tsuboi *et al*. (1995) and Kanamori & Rivera (2004), if $u(t)$ is the amplitude corrected, far-field, *P*-displacement for an earthquake source of duration T_0, then a theoretical expression for scalar seismic moment, M_0, is

$$M_0 = C_{\rm M} \int_{t_p}^{t_p+T_0} u(t)\mathrm{d}t. \tag{A1}$$

In the above expression t_p is the *P*-arrival time and $u(t)$ is corrected for geometrical spreading and attenuation. $C_{\rm M} = 4\pi \rho_{\rm s}{}^{1/2}\rho_{\rm r}{}^{1/2}\alpha_{\rm s}{}^{5/2}\alpha_{\rm r}{}^{1/2}Ff_{\rm s}$, where ρ and α are the density and *P*-wave speed, respectively, at the source s or the recording station r, and F and $f_{\rm s}$ are corrections for radiation pattern and free-surface amplification, respectively.

In this study, we use the 1-D, spherical, PREM model (Dziewonski & Anderson 1981) without a crust (PREM_NC) for amplitude correction of the displacement waveforms for attenuation and geometrical spreading. We choose PREM so that we can make unbiased comparisons with the global CMT results, which are based on PREM. In PREM_NC, the crustal layers are replaced by a layer with the PREM properties of the uppermost mantle; this eliminates unrealistic, discontinuous jumps in material properties and magnitude estimates at the crustal boundaries for small changes in the nominal hypocentre depth. Calculations are initially performed using ρ and α values for the uppermost mantle; later, for shallow continental events and deeper events (Table 1), the effect of the crust or event depth on ρ and α is re-introduced as a magnitude correction using the PREM properties at the depth of the event (Table 2).

The geometrical spreading is calculated from the spreading of rays between the source and station in the PREM_NC model using a standard expression (e.g. Aki & Richards 1980, eq. 9.44; Shearer 1999, eq. 6.23).

The attenuation correction is made in the frequency domain using standard relations (e.g. Shearer 1999; Lay 2002),

$$A_{\rm corr}(\omega) = A_0(\omega)\mathrm{e}^{-\omega t^*/2}, \tag{A2}$$

and,

$$t^* = \int_{\rm path} \frac{\mathrm{d}t}{Q\,(r)}, \tag{A3}$$

where $A_0(\omega)$ and $A_{\rm corr}(\omega)$ are the Fourier transforms of the initial and attenuation corrected displacements, and the integral in eq. (A3) is taken using the source–station ray path and corresponding Q values from the PREM_NC model.

If the integral in eq. (A1) includes all of the *P*-wave group (*P*, *pP* and *sP*) then the correction to displacement for radiation pattern is given by a factor $F = \sqrt{[<(F^P)^2>/(F^{gP})^2]}$ where $<(F^P)^2> = 4/15$ (e.g. Boatwright & Choy 1986) is the mean square radiation coefficient for *P* waves, and F^{gP} is a generalized radiation pattern coefficient for the *P*-wave group. For observations at teleseismic distances Newman & Okal (1998) suggest a constant value $F^{gP} = 1$ for the generalized radiation coefficient which is appropriate for dip-slip faulting but considered too high by as much as a factor of 4 for strike-slip faulting (Boatwright & Choy 1986; Choy & Boatwright 1995). This choice of F^{gP} gives $F = \sqrt{[\sqrt{<(F^P)^2>}]} = \sqrt{(4/15)} \approx 0.52$. However, if the integral in eq. (A1) includes only the direct *P* waves, then $F = [1/\sqrt{<(F^P)^2>}] = \sqrt{(15/4)} \approx 1.9$ (e.g. Tusboi *et al.* 1999) . Since in this study, we compensate for the presence of non-direct *P* waves by taking the integral in eq. (1) separately over the positive and negative displacement amplitudes, we use $F = \sqrt{(15/4)}$ for the radiation pattern correction for non-strike-slip events. Because of the ambiguity noted above in the radiation coefficients for strike-slip faulting, we determine empirically a magnitude correction for strike-slip events so that their M_{wpd} magnitudes best match $M_{\rm w}^{\rm CMT}$ on average (see Appendix B).

The correction for free-surface amplification at the station site introduces an additional factor of $f_{\rm s} = 1/2$. Incorporating the corrections for radiation pattern and free-surface amplification in $C_{\rm M}$, and using PREM_NC upper-mantle material properties for the source, $\rho_{\rm s} = 3.38\ \mathrm{g\,cm^{-3}}$, $\alpha_{\rm s} = 8.10\ \mathrm{km\,s^{-1}}$, and PREM upper crust properties for the recording stations, $\rho_{\rm r} = 2.60\ \mathrm{g\,cm^{-3}}$, $\alpha_{\rm r} = 5.80\ \mathrm{km\,s^{-1}}$, gives $C_{\rm M} = 1.62 \times 10^{19}$ when geometrical spreading is expressed as an equivalent source–station distance in units of km. The magnitude corrections to account for $\rho_{\rm s}$ and $\alpha_{\rm s}$ for shallow continental and deeper sources are listed in Table 2.

In the preceding, we have not directly accounted for the *PP* phase which arrives in the *P*-wave group and may be expected to bias the moment estimates upwards. However, the effect of *PP* on

the duration–amplitude magnitude calculations seems to be minor to insignificant, for three main reasons: (1) The majority of large events used in our study (69 out of 79) have duration $T_0 < 2$ min. For these events, *PP* at stations with GCD $> \sim 50^\circ$ arrives later than the window t_p to $t_p + T_0$ used for integration in eq. (A1). Thus, *PP* is for the most part not included in the calculation. Two of the few events where *PP* may be included in the integral are the 2004.12.26 M9.3 Sumatra–Andaman ($T_0 \approx$ 400–500 s) and the 2006.07.17 M7.7 Indonesia tsunami earthquake ($T_0 \approx 180$ s); but for both of these events raw M_{wpd} is less than $M_{\rm w}^{\rm CMT}$ and the moment corrected $M_{wpd} \approx M_{\rm w}^{\rm CMT}$, so there is no evidence of overestimation of $M_{\rm w}$ due to neglecting the effects of *PP*. (2) An examination of the displacement signals for longer duration ($T_0 > 2$ min) and larger events shows that the *PP* amplitudes are always smaller than the *P* amplitudes (e.g. Fig. 2, trace (3) exhibits a relatively large *PP* signal) and, for a majority of traces, are so small as to be difficult to identify. This phenomenon may be due to destructive interference of *PP* pulses for longer duration events, since *PP* is related to the Hilbert transform of the *P* waveform. The Hilbert transform of a simple pulse is a quasi-symmetric pair of positive and negative pulses. For the *PP* case, these two pulses are separated by a time interval that is much less than T_0 for the studied events, consequently there can be cancellation between positive and negative *PP* pulses originating from different subsources of the evolving rupture. (3) The moment magnitude is related to the logarithm of the moment (*cf.*, eq. 2; Fig. 2, traces 4 and 5), so a relatively large error in moment corresponds to a small error in magnitude (e.g. a factor of two error in M_0 leads to a change in $M_{\rm w}$ of 0.2).

APPENDIX B: DURATION–AMPLITUDE MOMENT AND MAGNITUDE CALCULATION

For each earthquake, we assume that we have a hypocentre location and predicted *P* and *S* traveltimes from the hypocentre to each recording station. Currently, most real-time monitoring agencies have this information within a few minutes after OT for local and regional events (GCD to stations $< \sim 30^\circ$), and within about 10–15 min of OT for teleseismic events (GCD to stations $> \sim 30^\circ$). We also assume that we have available vertical-component, broad-band, digital seismograms for about 20 or more stations at 30°–90° GCD from the source, and that these stations are moderately well distributed in distance and azimuth to avoid biases due to rupture directivity and other effects. We exclude from the analysis poor quality seismograms that are noisy, clipped, truncated or otherwise corrupted.

For the present study, we examine a set of recent earthquakes with a large range of magnitudes ($M_{\rm w}^{\rm CMT}$ 6.6–9.3) and diverse source types (Table 1). For each event, we obtain from the IRIS Data Management Center a set of broad-band vertical (BHZ) component recordings at stations from 30° to 90° GCD from the event. Typically we use about 20–50 records, selecting stations well distributed in distance for events which have more than 50 available records. All averages and standard deviations are obtained using robust statistics (i.e. 20 per cent trimmed—rejection of the upper and lower 20 percentiles of values), typically data from 15 to 45 stations are retained.

Duration determination

At teleseismic distance, direct *P* waves contain much more, higher-frequency energy than do other wave types such as *pP*, *sP*, *PP* or *S*. In consequence, the duration of the direct *P* waves and an apparent source duration, T_0, can be obtained from high-frequency seismograms (Lomax 2005; Lomax *et al.* 2007). We exploit this behaviour to estimate T_0 for each station using vertical-component seismograms, with the following procedure (see also Fig. 2), based on that of Lomax (2005) and Lomax *et al*. (2007): (1) Convert the seismograms from each station to high-frequency records using a narrow-band, Gaussian filter of the form $e^{-\alpha[(f - f_{\rm cent})/f]^2}$, where f is frequency, $f_{\rm cent}$ the filter centre frequency, and α sets the filter width. Here we use $f_{\rm cent} = 1.0$ Hz and $\alpha = 10.0$; as in Lomax (2005) and Lomax *et al*. (2007), in contrast to the 2–4 Hz bandpass filter used by Hara (2007). (2) Convert the high-frequency seismogram to velocity-squared time-series by squaring each of the data values. (3) Smooth the velocity-squared time-series with a 10 s wide, triangle function to form a station envelope function. (4) Measure the set of time delays after the *P* time at which the envelope function last drops below 90 (T^{90}), 80 (T^{80}), 50 (T^{50}) and 20 per cent (T^{20}) of its peak value. (5) Calculate the apparent source duration, T_0, for the station using the following algorithm,

$$T_0 = (1 - w)\, T^{90} + w T^{20}, \tag{B1}$$

where the weight $w = [(T^{80} + T^{50})/2 - 20\ \text{s}]/40$ s, with limiting values $0 \le w \le 1$.

The form of w and choice of 20 and 90 per cent of the envelope peak value to measure T_0 follow from examination of the shape of the summary envelope functions used in this study. In general, the 20 per cent peak value gives better agreement with published results for the larger events (e.g. $T_0 > 100$ s), while the 90 per cent peak value better results for the smallest events (e.g. $T_0 < 100$ s), in comparison to twice the CMT centroid time minus OT and other estimates of source duration. The necessity for different treatment of smaller and larger events is due to the longer length of the exponentially decaying, *P* coda in proportion to the source duration for smaller events than for larger events.

We also calculate an average T_0 and associated standard deviation for each event by taking the geometric mean and geometric standard deviation of the station T_0 estimates using robust statistics (i.e. 20 per cent trimmed measures).

In general, the duration–amplitude T_0 estimates are greater than twice the CMT centroid time minus OT (*cf.* Table 1), since the T_0 estimation procedure accounts well for the very long and complex rupture of larger events (which are not well represented by the single-triangle source function used in CMT), while T_0 will tend to overestimate the durations for smaller events due to problems with the relatively long coda in the high-frequency seismograms.

Duration–amplitude moment and magnitude calculation

We evaluate the seismic moment, M_0^{pd}, for each station using vertical-component seismograms and the following procedure (see also Fig. 2): (1) Bandpass from 1 to 200 s (see Appendix C), remove the instrument response and apply geometrical spreading and attenuation corrections to convert each seismogram to amplitude corrected, ground displacement. (2) Cut each seismogram from 10 s before the *P*-arrival to the *P*-arrival time plus the source duration, T_0, or to 10 s before the *S* arrival, whichever is earlier, to obtain *P*-wave seismograms. (3) Apply eqs (3) and (5a or 5b) to each *P*-wave seismograms to obtain station moment estimates. (4) Multiply the station moment value by a factor T_0/t_{S-P} if $T_0 > t_{S-P}$, where t_{S-P} is the *S*-arrival time minus the *P*-arrival time. We calculate an average M_0^{pd} and associated standard deviation for each event by taking the geometric mean and geometric standard deviation of the station moment estimates using robust statistics

(i.e. 20 per cent trimmed—rejection of the upper and lower 20 percentiles of values). We calculate the duration–amplitude magnitude, M_{wpd}, through application of the standard moment to moment-magnitude relation (Hanks & Kanamori 1979; Bormann 2002),

$$M_{wpd} = \left(\log_{10} M_0^{pd} - 9.1\right)/1.5, \quad \text{(B2)}$$

where M_0^{pd} has units of N-m.

We include a constant, k, in eq. (3) to compensate for the errors and biases in the geometrical spreading and attenuation corrections and in the terms of C_M. We evaluate k through comparison of our M_0^{pd} values for each event against the corresponding CMT moment values, M_0^{CMT}, so that the mean of $\log_{10}(M_0^{pd}/M_0^{CMT}) \rightarrow 0$, giving $k \approx 1.2$. This evaluation excludes interplate thrust, tsunami and strike-slip events and 2002 November 3 Alaska (labelled RS in plots) which has an unstable T_0 estimate due to exceptional source complexity (e.g. Fuis & Wald 2003). We use only interplate thrust and tsunami events to determine the constant $M_0^{cut-off}$ in eq. (5a), giving $M_0^{cut-off} \approx 7.5 \times 10^{19}$ N - m (equivalent to $M_w \approx 7.2$), and to determine the optimal value of R in eq. (4) by minimizing the standard deviation of $\log_{10}(M_0^{pd}/M_0^{CMT})$, giving $R \approx 0.45$. The optimal values of $M_0^{cut-off}$ and R are sensitive to details of the algorithms used to estimate T_0 and moment; a change of ± 0.25 in R gives about half the variance reduction relative to $R = 0$ (i.e. no moment scaling) than gives $R \approx 0.45$. The empirically determined magnitude correction to account for the radiation pattern of strike-slip events (types S and So in Table 1) has a value of 0.13 magnitude units; this value implies that for strike-slip events an additional factor of about 1.6 is needed in the correction for radiation pattern, F, in eq. (A1).

APPENDIX C: DEPENDENCE OF DURATION–AMPLITUDE RESULTS ON LONG-PERIOD CUT-OFF

The values of moment and of moment magnitude, M_{wpd}, for large events obtained with the duration–amplitude procedure depend on the long-period cut-off used when processing the seismograms. Indeed, it is generally accepted that magnitude saturation, regardless of the magnitude estimation technique, is related to the long-period data cut-off being lower than a corner period above which the displacement spectrum flattens to an amplitude proportional to the static moment (e.g. Stein & Okal 2007). Magnitude saturation also arises for methods that use a signal duration after the initial P arrival that is shorter than the duration of significant P signal and the source duration (e.g. Granville *et al.* 2005); the duration–amplitude procedure avoid this latter problem by explicitly taking into account the source duration.

Fig. C1 shows duration–amplitude magnitudes, M_{wpd}, with no moment scaling, for the seven largest and one tsunami earthquake from the studied events, plotted as a function of long-period cut-off, $T_{cut-off}$. With increasing $T_{cut-off}$ to about 50 s, there is an increase in magnitude estimates for all events; this increase can be associated with magnitude saturation due to $T_{cut-off}$ being lower than the long-period spectral corner for P waves. However, at around $T_{cut-off} = 50$–200 s the curves in Fig. C1 flatten and the magnitude estimates are nearly independent of $T_{cut-off}$, indicating that the long-period corner for P waves for each event has been reached and that the resulting magnitude estimates should not be saturated. Above around $T_{cut-off} = 200$ s, the magnitude estimates again increase with $T_{cut-off}$; examination of the processed seismograms shows that this increase is primarily an artefact of amplification of long-period noise in the P-wave train during the removal of the instrument response. The onset of P-wave noise above about 200 s period is expected since the typical long-period corner is about 120–360 s for the very-broad-band instruments providing much of the data used in this study.

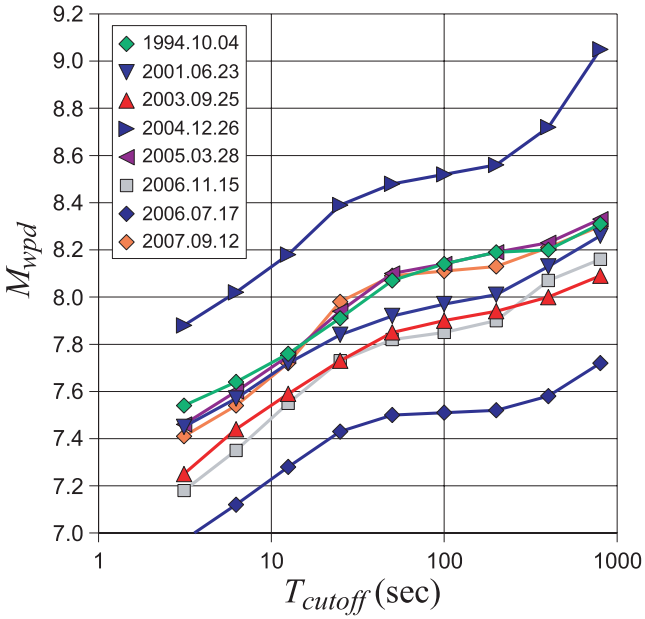

Figure C1. Duration–amplitude magnitudes, M_{wpd}, with no moment scaling (i.e. application of eq. 3) for the seven largest and one tsunami earthquake (2006.07.17 Indonesia) from the studied events (Table 1) plotted as a function of long-period cut-off used for analysis. The events are identified by their origin dates.

These results and Fig. C1 indicate that (1) The optimal long-period cut-off for the studied data set is 100–200 s. (2) The trend of increasing underestimate of M_w^{CMT} by unscaled M_{wpd} with increasing M_w^{CMT} (Fig. 3) cannot be attributed to a magnitude saturation problem due to insufficient, long-period signal.